THE ASTROPHYSICAL JOURNAL, 534:825–837, 2000 May 10

THE THREE-DIMENSIONAL STRUCTURE OF THE WARM LOCAL INTERSTELLAR MEDIUM. II. THE COLORADO MODEL OF THE LOCAL INTERSTELLAR CLOUD[1]

SETH REDFIELD AND JEFFREY L. LINSKY
JILA, University of Colorado and NIST, Campus Box 440, Boulder, CO 80309-0440; sredfiel@casa.colorado.edu
Received 1999 April 26; accepted 1999 December 28

ABSTRACT

In this second paper in a series on the structure of the local interstellar medium (LISM), we construct a three-dimensional model of the local interstellar cloud (LIC) based on *Hubble Space Telescope* (*HST*), *Extreme Ultraviolet Explorer* (*EUVE*), and ground-based Ca II spectra. Starting with hydrogen column densities derived from deuterium column densities measured with the Goddard High Resolution Spectrograph instrument on *HST* for 16 lines of sight to nearby stars, we derive a model consisting of the sum of nine spherical harmonics that best fit the data. We then rederive the model by including the lines of sight to three hot white dwarfs observed by *EUVE* and 13 lines of sight with Ca II column densities at the projected LIC velocity. The LIC model is clearly not a long thin filamentary structure like optical images of some interstellar clouds (e.g., reflection nebulae in the Pleiades), but neither is it spherical in shape. As seen from the north Galactic pole, the LIC is egg-shaped with an axis of symmetry that points in the direction $l \approx 315°$. Since the direction of the center of the Scorpius-Centaurus association is $l = 320°$, the shape of the LIC could be determined by the flow of hot gas from Sco-Cen. The model shows that the Sun is located just inside the LIC in the direction of the Galactic center and toward the north Galactic pole. The absence of Mg II absorption at the LIC velocity toward α Cen indicates that the distance to the edge of the LIC in this direction is ≤ 0.05 pc and the Sun should cross the boundary between the LIC and the Galactic (G) cloud in less than 3000 yr. We estimate that the volume of the LIC is about 93 pc^3 and its mass is about 0.32 $M_\odot$. The physical parameters and hydrogen column density of the LIC are roughly consistent with theoretical models of the warm interstellar medium that assume pressure and ionization equilibrium. However, the empirical hydrogen ionization of the LIC is much higher and the gas temperature lower than the theoretical models predict. Therefore, the ionization is likely due to shock activity from a nearby supernova that has not yet reached equilibrium. The higher ionization increases the gas cooling, which can explain why the gas is 2400 K cooler than the ionization equilibrium models predict. Computed and observed temperatures are in agreement for a model with the observed LIC electron density.

Subject headings: circumstellar matter — dust, extinction — infrared: ISM: lines and bands — ISM: abundances — molecular processes

1. INTRODUCTION

In their classic paper, Field, Goldsmith, & Habing (1969) proposed that thermal instability naturally leads to a multiphase interstellar medium (ISM) in which the individual phases coexist at constant pressure. They identified two phases (cold and warm) in their rather quiescent model of the interstellar medium. Cox & Smith (1974) identified a third phase in the constant pressure ISM: hot gas energized by supernovae. Over the years, these models have been modified by including new heating, cooling, ionization, and recombination rates, together with additional physical processes including cloud evaporation and thermal conduction. Cox & Reynolds (1987) and McKee (1995) provide comprehensive summaries of this topic. In recent terminology, the phases of the interstellar medium are called CNM (cold neutral medium), WNM (warm neutral medium), WIM (warm ionized medium), and HIM (hot ionized medium).

While theory often provides useful prototypes and insights into the essential physics, theoretical models are always simplifications. In particular, pressure equilibrium among the different phases, ionization equilibrium within a phase, and standard values for illuminating radiation fields and grain absorption may not be representative of real interstellar gas. Observations, therefore, are required to test the theory and provide guidance on how it should be modified.

Lallement & Bertin (1992) and Lallement et al. (1995) demonstrated that the Sun lies inside a warm, partially ionized, low-density cloud which they called the local interstellar cloud (LIC). This cloud is part of a complex of warm clouds that is located either inside or at the edge of a superbubble (called the Local Bubble) produced by the OB star winds and supernovae of the Scorpius-Centaurus association (Frisch 1995; Lyu & Bruhweiler 1996). Linsky et al. (2000, hereafter Paper I) summarize the hydrogen and deuterium column densities through the LIC along many lines of sight toward nearby stars inferred from spectra obtained with the Goddard High Resolution Spectrograph (GHRS) and Space Telescope Imaging Spectrograph (STIS) instruments on the *Hubble Space Telescope* (*HST*) and the *Extreme Ultraviolet Explorer* (*EUVE*), respectively. With accurate absorption-line data for these many lines of sight, measurements of the LIC gas flowing through the solar system, and knowledge of the far-UV radiation illuminating the LIC from surrounding stars, we surely know more about the LIC than any other interstellar cloud. Comparison of the LIC with recent theoretical models (Wolfire et al.

[1] Based on observations with the NASA/ESA *Hubble Space Telescope*, obtained at the Space Telescope Science Institute, which is operated by the Association of Universities for Research in Astronomy, Inc., under NASA contract NAS 5-26555.

1995a), therefore, can provide an excellent test of these models.

In this second paper in our series on the structure of the local interstellar medium (LISM), we construct two three-dimensional models of the LIC based on GHRS, *EUVE*, and Ca II spectra.[2] The first model is based exclusively on the very best GHRS, STIS, and *EUVE* data available (data set A). The second model is based on as many reliable sight lines as is possible, including GHRS, STIS, *EUVE*, and Ca II data (data set B). A comparison of these two models will give a measure of the stability and robustness of our modeling. These models turn out to be closer in shape to a sphere than to a thin sheet, which is often thought to be the preferred geometry of warm clouds. With the morphology and physical properties of our LIC model now reasonably well known, we can compare the LIC with theoretical models for the same input parameters. We can also compare the LIC morphology with the directions of the incoming gas flows and radiation fields to search for empirical evidence that may identify the physical processes that control the cloud's shape.

2. ASTRONEPHOGRAPHY: THE SURFACE OF THE LIC

2.1. *Fitting the HST Data Set*

In Paper I several strong arguments are made that the most accurate way to derive hydrogen column densities for lines of sight through the LIC is to multiply the deuterium column densities measured in GHRS and STIS spectra by the mean D/H ratio in the LIC, 1.5×10^{-5}. The distance from the outer edge of the heliosphere to the edge of the LIC, in units of parsecs, $d_{\rm edge}$(LIC), along a given line of sight is then derived using $d_{\rm edge}({\rm LIC}) = N_{\rm H\,I}({\rm LIC})/3.086 \times 10^{18} n_{\rm H\,I}$. We assume that the interstellar gas moving with the LIC speed has a constant density, $n_{\rm H\,I} = 0.10$ cm^{-3}, since the largest mean density along nearby lines of sight is 0.10 cm^{-3}. We also assume that the LIC is uniformly filled with gas.

Our data set consists of the Galactic coordinates (l, b) and values of $d_{\rm edge}$(LIC) toward the 16 stars for which we have deuterium column densities (or upper limits) obtained from GHRS and STIS spectra. In the case of upper limits, we set $d_{\rm edge}$(LIC) equal to the upper limit. To describe the LIC in three dimensions, we use a function that requires only the three spherical coordinates, θ, ϕ, and r, where θ and ϕ are the Galactic coordinates of the star and r is the distance to the edge of the LIC in units of parsecs, as discussed in Paper I. If in fact the shape of the LIC is quasi-spherical, the use of spherical harmonics as the orthogonal set of basis functions seems appropriate. We make no prior assumptions regarding the shape or smoothness of the LIC. With enough spherical harmonics, it is possible to produce any arbitrary closed surface. The quality of the fits and reproducibility of a similar LIC shape lead us to claim that such a quasi-spherical shape may describe the three-dimensional structure of the LIC. We fit this data set with a sum of spherical harmonics with the amplitudes and orientations calculated with a least-squares routine. Spherical harmonics are a useful set of orthogonal basis functions because they can accommodate a wide range of surface shapes and orientations. The specific mathematical form of the spherical harmonics is discussed in detail in the Appendix.

The construction of the model required us to define a Cartesian coordinate system to map the data onto the spherical coordinate system that our fitting routine operates in. We chose the most obvious and convenient coordinate system with the Sun at the origin, the z-direction toward the north Galactic pole, the x-direction toward the Galactic center, and the y-direction toward Galactic east. Although the LIC has no preferred coordinate system, the spherical harmonics used in the fitting routine do. For all spherical harmonics with $l > 0$, the z-direction is an axis of orientation. Therefore, for each individual data set discussed in this paper we fit three different sets of spherical harmonics, based on three different axes of orientation. These orientations are as follows: (1) the z-direction corresponds to the north Galactic pole direction; (2) the z-direction corresponds to the direction toward the Galactic center, which is also the direction toward the Galactic (G) cloud and essentially the axis from the center of the cloud to the Sun; and (3) the z-direction corresponds to Galactic east, a halfway point between the largest and shortest extent of the LIC. With a very large number of data points, the orientation of the spherical harmonics would be irrelevant and each orientation would produce the same result. With few data points and portions of the sky poorly sampled, however, the orientation can affect the final shape, as different regions are sampled by different order harmonics.

Our proposed LIC model is based on the average of these three models with different orientations. This technique of orientation-averaging allows us to create the most general solution to the three-dimensional structure of the LIC, as well as to easily identify regions where our model is either well constrained or poorly constrained. Figure 1 is an example of this orientation-averaging technique for data sets A and B (the contents of these data sets will be discussed below). For each data set, the solid line contour is the weighted average of the nonsolid line contours, which represent individual models based on different orientations. The examples in Figure 1 also provide some insight into the error involved in our model. Our model is an excellent fit to the data in the direction toward Galactic center and Galactic north, as all models give the same result in those directions, regardless of orientation. However, our model is poorly constrained in the direction of Galactic anticenter, where the models differ by parsecs. There are no data points in that direction that correspond to the 0 pc contour, as seen from Galactic west, to constrain the models, so each orientation fits it differently. Our three-dimensional models of the LIC will therefore be produced by this average-orientation technique. In the final contour maps of the model, we will distinguish areas which are well constrained from areas which are poorly constrained based on the results of the different orientations.

Our procedure is first to fit a sphere to the 16 *HST* data points by a least-squares method. We then add successively more spherical harmonics. As we add more harmonics and thus sample the LIC shape with finer and finer structures, the fit of the sum of the harmonics to the data points has increasing accuracy (decreasing values of reduced χ^2). For

[2] The resulting model can be viewed at the Colorado Model of the Local Interstellar Medium Web site, http://casa.colorado.edu/~sredfiel/ColoradoLIC.html. The input data, the prescription for computing the model, and a tool for calculating the hydrogen column density through the LIC along any line of sight will also be available at this Web site. As new data appear, the Web site will include new versions of the LIC model and models for nearby warm clouds in the LISM.

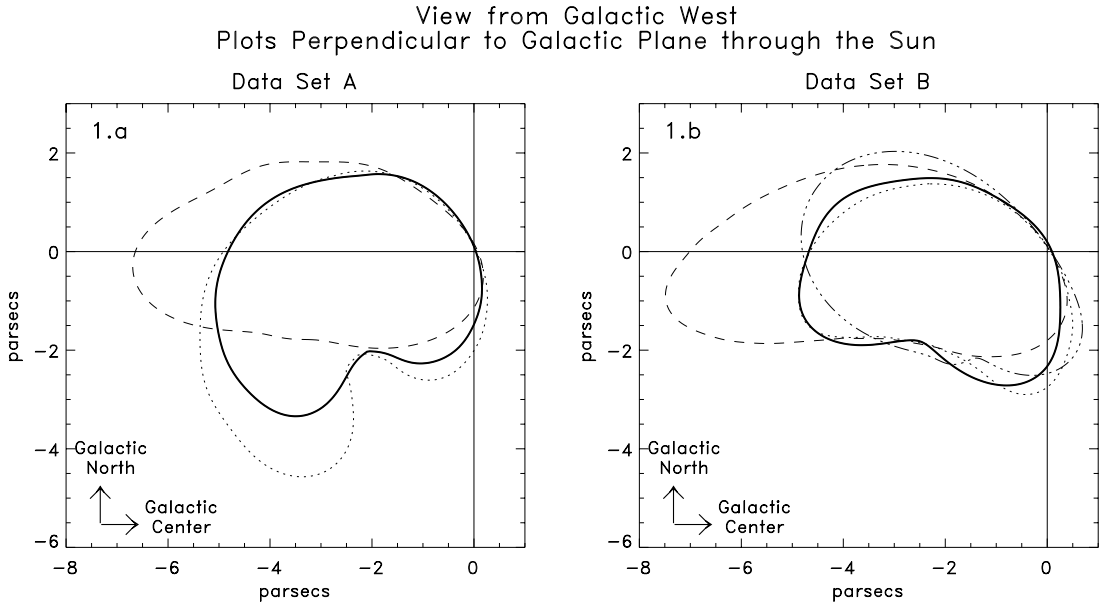

FIG. 1.—(*a*) View from Galactic west ($l = 270°$, $b = 0°$) of various LIC models computed from hydrogen column densities inferred from *HST* and *EUVE* spectra (data set A). The Sun is located at (0,0), and the directions toward the Galactic center ($l = 0°$) and Galactic north ($b = 90°$) are indicated. The nonsolid lines indicate models derived from spherical harmonics at different orientations (*dotted line*: *z*-direction corresponds to north Galactic pole; *dashed line*: *z*-direction corresponds to Galactic center). The model associated with an orientation of the *z*-direction to Galactic east did not produce a realistic solution because of the limited number of data points. The thick solid line indicates the final model for data set A, derived from the weighted average of all orientations. (*b*) Same view as (*a*) except for data set B. Here all orientations are present, as there are more data points available to constrain the model (*dotted line*: *z*-direction corresponds to north Galactic pole; *dashed line*: *z*-direction corresponds to Galactic center; *dash-dotted line*: *z*-direction corresponds to Galactic east). Although both data set A and data set B produce similar models for the LIC, notice the improvement in the model for data set B as a result of the inclusion of the Ca II data points. The model (*solid line*) is now well constrained in almost every direction except toward Galactic anticenter. This figure helps visualize the average-orientation technique used to construct our final three-dimensional models of the LIC.

each harmonic ($y_{l,m}$), we determine the corresponding amplitude (the $a_{l,m}$ coefficient, see the Appendix) by minimizing χ^2. This coefficient is proportional to the importance of that harmonic to successfully fitting the shape of the LIC. As we will see from the value of the $a_{0,0}$ coefficient, the $y_{0,0}$ harmonic (the sphere) is clearly the predominant shape associated with the LIC. We expect the remaining $y_{l,m}$ values to be less important than the $y_{0,0}$ harmonic, and therefore $a_{l>0,m} < a_{0,0}$. However, we do not expect the $a_{l,m}$ values to necessarily decrease monotonically with increasing l, which would be the case only when the LIC data points lie on a surface that is close to a sphere. A larger or smaller coefficient simply indicates the relative importance of the corresponding harmonic to the overall shape of the LIC. Typically, we can fit the LIC to order 9 ($l = 0, 1, 2$) before the model starts computing negative or unrealistically large distances from the center of the model to some directions between the data points. It is for this reason that Figure 1*a* contains only two (instead of three) different orientation models. The orientation associated with the *z*-direction toward Galactic east does not produce a realistic solution. The data set used for Figure 1*a* contains only 17 data points, whereas the data set used in Figure 1*b* has 32 data points. When we added more data points in creating data set B, the problem disappeared and the third orientation was sufficiently constrained to produce a satisfactory solution.

2.2. *Fitting the EUVE Data Set*

We next considered whether the hydrogen column densities toward the white dwarfs observed by *EUVE* are consistent with the LIC shape determined only with the *HST* data. Since the *EUVE* hydrogen column densities refer to the absorption by all clouds in the line of sight, we do not know a priori whether the lines of sight to any of these stars pass through only the LIC. The value of $d_{\rm edge}$ for only one of the *EUVE* targets (GD 50) is accurately fit with the LIC shape. For this nearby star (37 pc), $N_{\rm H\,I}$(total) is similar to the values of $N_{\rm H\,I}$(LIC) determined from GHRS spectra for the stars HR 1099, ϵ Eri, and 40 Eri A that lie between 3°.4 and 11° from GD 50 on the sky. We therefore include GD 50 in our list of lines of sight and rederive the LIC shape based on what we call data set A (16 *HST* lines of sight plus GD 50).

Table 1 shows the fits to the model LIC using 16 *HST* data points and one *EUVE* data point (GD 50). Using data set A, we find that the center of the LIC is located at $(x, y, z) = (-2.2, +1.2, -1.1)$, where x is the distance (parsecs) from the Sun toward the Galactic center, y is the distance (parsecs) from the Sun toward Galactic east ($l = 90°$), and z is the distance (parsecs) from the Sun toward the north Galactic pole. Thus, the center of the model lies away from the Galactic center and toward Galactic east and the south Galactic pole.

For each line of sight, $d_{\rm edge}$ is the distance from the Sun to a point P that is at the edge of the LIC. The distance from the center of the LIC model to point P is $d_{\rm obs}$, and $d_{\rm model}$ is the distance from the center of the LIC model to the edge of the LIC model in the direction of point P. In Table 1 we list for the 17 lines of sight the values of $d_{\rm obs}$, $d_{\rm model}$, and the difference between these two quantities, $d_{\rm model} - d_{\rm obs}$. All of these quantities are in parsecs. Column (7) in the table lists the relative weight of each data point that is inversely proportional to the uncertainty in the measured $N_{\rm H\,I}$(LIC). For

this LIC model, the average difference between $d_{\rm model}$ and $d_{\rm obs}$ is 0.14 pc and the reduced $\chi^2 = 0.56$. The table also includes lines of sight toward two white dwarfs (GD 71 and V471 Tau) and 13 Ca II stars (see below) that were not included in the model fit by giving them zero weight. Note that the two white dwarfs have differences ($d_{\rm model} - d_{\rm obs}$) of about +0.8 pc, indicating that the shape of the LIC created using data set A is too large in their direction. Also note that practically all the Ca II stars seem to fit fairly well, with an average difference of only 0.43 pc. We will use all of these stars in data set B, in order to test the robustness of our model. The two white dwarfs should be included in order to constrain the model because they provide upper limits to the edge of the LIC in those directions. The Ca II stars should be added in order to provide more lines of sight and a more stable and robust model. These additions are included in data set B and will be discussed shortly.

2.3. *Fitting the* Ca II *Data Set*

We now compare the model for the LIC obtained only from neutral hydrogen absorption, data set A (16 *HST* stars and one *EUVE* star), with a larger data set of interstellar absorption by a trace element. Large ground-based surveys of interstellar absorption in the Na I and Ca II resonance lines are now available, but we believe that the Ca II K–line data provide a better tracer of local warm interstellar gas because strong Na I absorption is observed in cold clouds and many more stars within 50 pc show Ca II absorption than Na I absorption. In particular, Génova et al. (1997) note that nearby stars with Ca II absorption at the predicted velocities of the LIC and G clouds rarely show Na I absorption at these velocities. Three high spectral resolution surveys of Ca II absorption toward some 120 stars (Vallerga et al. 1993; Welty, Morton, & Hobbs 1996; Crawford 1991) are available, as well as a few observations at 0.3 km s^{-1} resolution (Crawford & Dunkin 1995).

We list in Table 2 the data for the 14 stars in these surveys that show Ca II absorption at the projected LIC velocity. Our criteria for selection are that the measured velocities lie within 0.7 km s^{-1} of the predicted velocity, that the measured broadening parameter $b_{\rm Ca\ II}$ be at least as large as that expected for a temperature of 7000 K, and that the star not be in the general direction of the G cloud, which is tentatively set as within 40° of α Oph ($l = 36°$, $b = +22°$). For our analysis of the LIC, we include all stars within 100 pc that meet these criteria.

TABLE 1

COMPARISON OF LIC MODEL WITH GHRS AND *EUVE* DATA

Star Symbol (1)	Star Name (2)	d (pc) (3)	l (deg) (4)	b (deg) (5)	$d_{\rm obs}$ (pc) (6)	Weight (7)	$d_{\rm model}$ (pc) (8)	$d_{\rm model} - d_{\rm obs}$ (pc) (9)
Stars Included in the Model Fit								
αC	α Cen	1.35	316	−01	2.744	2.0	2.729	−0.015
SI	Sirius	2.63	227	−09	2.588	2.7	2.776	+0.188
ϵE	ϵ Eri	3.22	196	−48	1.811	6.7	1.764	−0.047
61	61 Cyg A	3.48	082	−06	2.527	6.7	2.565	+0.038
PR	Procyon	3.50	214	+13	2.887	9.1	2.922	+0.035
40	40 Eri A	5.04	201	−38	1.883	4.8	1.878	−0.005
βG	β Gem	10.3	192	+23	3.183	4.8	2.949	−0.234
CA	Capella	12.9	163	+05	4.154	9.1	3.700	−0.454
βC	β Cas	16.7	118	−03	3.377	9.1	3.113	−0.264
αT	α Tri	19.7	139	−31	1.497	4.8	2.085	+0.588
99	HR 1099	29.0	185	−42	1.496	9.1	1.505	+0.009
43	HZ 43	32.0	054	+84	2.843	2.0	2.755	−0.088
σG	σ Gem	37.5	191	+23	2.907	4.8	2.969	+0.062
G1	G191−B2B	68.8	156	+07	3.519	4.4	3.864	+0.345
31	31 Com	94.2	115	+89	2.743	7.7	2.741	−0.002
ϵC	ϵ CMa	132	240	−11	2.750	2.0	2.736	−0.014
50	GD 50	37	187	−39	1.556	22.	1.536	−0.020
Stars Excluded from the Model Fit								
71	GD 71	46.5	192	−05	2.029	0.0	2.698	+0.669
V4	V471 Tau	46.8	172	−28	2.445	0.0	3.326	+0.881
αQ	α Aql	5.1	048	−9	3.024	0.0	2.589	−0.435
αP	α PsA	7.7	020	−65	2.715	0.0	2.616	−0.099
AC	α Cep	15.0	101	+09	2.368	0.0	2.579	+0.211
βP	β Pic	19.3	258	−31	3.044	0.0	2.498	−0.546
δV	δ Vel	24.4	272	−07	3.233	0.0	2.705	−0.528
δC	δ Cas	30	127	−02	2.146	0.0	2.688	+0.542
αA	α And	30	112	−33	1.891	0.0	1.943	+0.052
αG	α Gru	31	350	−52	3.127	0.0	2.586	−0.541
αL	α Lac	31	101	−07	2.138	0.0	2.497	+0.359
AP	α Peg	43	088	−40	2.363	0.0	2.408	+0.045
γA	γ Aqr	48	062	−46	2.640	0.0	2.565	−0.075
ηQ	η Aqr	56	067	−48	3.774	0.0	2.358	−1.416
ηA	η Aur	67	165	+00	2.104	0.0	2.811	+0.707

In order to derive values of $d_{\rm edge}$ from measurements of $N_{\rm Ca\,II}$, we must know the abundance ratio $N_{\rm Ca\,II}/N_{\rm H\,I}$ in the LIC. Because this ratio can vary by a factor of 10 among different interstellar clouds and is therefore the greatest contributor of error for the Ca II estimates of $d_{\rm edge}$, we make this ratio a free parameter in our model. For all three orientations, we allow the $N_{\rm Ca\,II}/N_{\rm H\,I}$ ratio to vary and determine the best-fit value and errors based on the least χ^2 criterion. For the orientation of the z-direction corresponding to the north Galactic pole, we obtain a $N_{\rm Ca\,II}/N_{\rm H\,I} = 2.34^{+0.89}_{-0.41} \times 10^{-8}$, for the z-direction corresponding to the Galactic center $N_{\rm Ca\,II}/N_{\rm H\,I} = 2.19^{+0.50}_{-0.01} \times 10^{-8}$, and for the final orientation where the z-direction corresponds to Galactic east $N_{\rm Ca\,II}/N_{\rm H\,I} = 2.36^{+1.21}_{-0.75} \times 10^{-8}$. It is encouraging that the $N_{\rm Ca\,II}/N_{\rm H\,I}$ ratio is independent of orientation, as all three give consistent results. The mean abundance ratio based on these results is $N_{\rm Ca\,II}/N_{\rm H\,I} = 2.30^{+0.53}_{-0.28} \times 10^{-8}$, which is similar to the mean ratio $N_{\rm Ca\,II}/N_{\rm H\,I} = 1 \times 10^{-8}$ that Frisch (1996) finds is typical of warm neutral clouds. The $N_{\rm H\,I}$ values listed in Table 2 are based on the $N_{\rm Ca\,II}/N_{\rm H\,I} = 2.30^{+0.53}_{-0.28} \times 10^{-8}$ abundance ratio, and all models based on Ca II data will use this value to derive $d_{\rm edge}$ for each line of sight. Table 2 lists the derived hydrogen column densities, mean hydrogen number densities, and distances to the edge of the LIC for these lines of sight. Note that for all lines of sight the inferred value of $\langle n_{\rm H\,I} \rangle < 0.1$ cm^{-3}, so that all of the stars lie outside of the LIC.

Since the models computed with and without the Ca II lines of sight are in very good agreement where there are an adequate number of data points, we are confident that we can include Ca II column densities in models for the LIC and other nearby warm clouds. Figure 1 compares the results of data set A and data set B (which includes Ca II). It is clear that the results are strikingly similar and that the addition of the Ca II lines of sight significantly improves the consistency among the models computed with different orientations. Note the good agreement in Figure 1*b* among the three models toward the south Galactic pole where there are a number of Ca II data points but no *HST* or *EUVE* data points. With the additional constraints provided by the Ca II data points, we also felt confident in adding two more *EUVE* white dwarfs (GD 71 and V471 Tau). These stars show hydrogen column densities consistent with interstellar absorption only from the LIC and so can therefore be added to further constrain the LIC model. Table 3 shows the fits to the model LIC using 16 *HST* data points, three *EUVE* data points, and 13 Ca II data points. We refer to these data as data set B. Previously, the total hydrogen column density for GD 71 and V471 Tau placed them about 0.8 pc inside the boundary of the LIC computed from data set A. Including them in the calculation now places them only about 0.6 pc inside the LIC model, which is probably consistent with the measurement errors. The reduced $\chi^2 = 1.33$, and the average difference between $d_{\rm model}$ and $d_{\rm obs}$ is 0.28 pc. The model center is now $(x, y, z) = (-2.5, 1.5, -1.5)$. Table 4 compares the parameters for the models based on data sets A and B, and it also lists the spherical harmonic coefficients, as discussed in the Appendix, derived for both models.

2.4. *Visualizing the LIC Model*

Figures 2–4 provide views of the LIC models created from the sum of nine spherical harmonics that best fit data set B. Figure 2 shows the LIC model based on data set B as viewed from the north Galactic pole ($b = +90°$). The 0 pc line shows the edge of the LIC in a plane through the Sun that is parallel to the Galactic plane. The -2 and -4 pc lines show parallel planes (at 2 pc increments) south of the Sun. Solid lines indicate where the three different orientations agree very well, and we feel the model is well constrained. The dotted line regions indicate where the model is poorly constrained, as indicated by the three orientation models disagreeing with each other by greater than a few tenths of a parsec. The crosshairs at the origin indicate the location of the Sun. The Sun is located very close to the edge of the LIC, and the main axis of the egg-shaped model faces toward $l = 315°$, close to the direction of the center of the Sco-Cen association.

TABLE 2

Ca II Column Densities and Distances to the Edge of the LIC

Star Symbol (1)	Star Name (2)	d (pc) (3)	l (deg) (4)	b (deg) (5)	$v_{\rm LIC}$ (km s^{-1}) (6)	$v_{\rm obs}$ (km s^{-1}) (7)	$b_{\rm Ca\,II}$ (km s^{-1}) (8)	$N_{\rm Ca\,II}$ ($\times 10^{10}$) (9)	$N_{\rm H\,I}$[a] ($\times 10^{18}$) (10)	$\langle n_{\rm H\,I} \rangle$ (cm^{-3}) (11)	$d_{\rm edge}$ (pc) (12)	Reference (13)
αQ	α Aql	5.1	48	−09	−17.0	−17.4	2.0	0.72	0.31	0.020	1.01	1
αP	α PsA	7.7	20	−65	−3.5	−3.2	...	0.55	0.24	0.010	0.77	2
AC	α Cep	15.0	101	+9	+0.9	+0.2	1.7	0.7	0.30	0.007	0.97	3
βP	β Pic	19.3	258	−31	+10.3	+10.8	...	1.0	0.43	0.007	1.41	2
δV	δ Vel	24.4	272	−07	+2.2	+2.5	...	0.71	0.31	0.004	1.00	4
δC	δ Cas	30	127	−02	+12.9	+12.3	...	0.5	0.22	0.002	0.70	3
αA	α And	30	112	−33	+9.6	+8.9	3.9	2.3	1.00	0.011	3.24	5
αG	α Gru	31	350	−52	−8.5	−8.0	...	0.5	0.22	0.002	0.70	3
		...	...	...	...	−10.2	2.3	1.1	0.48	0.005	1.55	6
αL	α Lac	31	101	−07	+3.0	+3.5	1.6	1.0	0.43	0.005	1.41	3
AP	α Peg	43	88	−40	+2.0	+2.0	1.9	1.7	0.74	0.006	2.40	3
γA	γ Aqr	48	62	−46	−4.4	−4.5	2.0	1.1	0.48	0.003	1.55	3
		...	...	...	...	−4.4	2.9	0.9	0.39	0.003	1.27	5
κA	κ And	52	110	−17	+7.8	+7.6	6.3	6.1	2.65	0.017	8.60	5
ηQ	η Aqr	56	68	−48	−2.4	−2.1	3.3	2.7	1.17	0.007	3.80	5
ηA	η Aur	67	165	+00	+23.0	+23.0	1.9	0.5	0.22	0.001	0.70	3

References.—(1) Ferlet, Lallement, & Vidal-Madjar 1986; (2) Lallement et al. 1995; (3) Lallement & Bertin 1992; (4) Lallement, Vidal-Madjar, & Ferlet 1986; (5) Vallerga et al. 1993; (6) Crawford & Dunkin 1995.

[a] $N_{\rm Ca\,II}/N_{\rm H\,I} = 2.30^{+0.53}_{-0.28} \times 10^{-8}$; see text.

TABLE 3

COMPARISON OF LIC MODEL WITH GHRS, *EUVE*, AND Ca II DATA

Star (1)	d (pc) (2)	l (deg) (3)	b (deg) (4)	d_{obs} (pc) (5)	Weight (6)	d_{model} (pc) (7)	$d_{model} - d_{obs}$ (pc) (8)
α Cen	1.35	316	−01	3.265	2.0	3.268	+0.003
Sirius	2.63	227	−09	3.128	2.7	3.328	+0.200
ϵ Eri	3.22	196	−48	2.162	6.7	2.428	+0.266
61 Cyg A	3.48	082	−06	2.971	6.7	3.029	+0.058
Procyon	3.50	214	+13	3.392	9.1	3.393	+0.001
40 Eri A	5.04	201	−38	2.271	4.8	2.510	+0.239
β Gem	10.3	192	+23	3.566	4.8	3.374	−0.192
Capella	12.9	163	+05	4.000	9.1	3.518	−0.482
β Cas	16.7	118	−03	3.159	9.1	2.764	−0.395
α Tri	19.7	139	−31	0.978	4.8	1.295	+0.317
HR 1099	29.0	185	−42	1.759	9.1	1.994	+0.235
HZ 43	32.0	054	+84	3.370	2.0	3.268	−0.102
σ Gem	37.5	191	+23	3.325	4.8	3.404	+0.079
G191-B2B	68.8	156	+07	3.388	4.4	3.605	+0.217
31 Com	94.2	115	+89	3.267	7.7	3.270	+0.003
ϵ CMa	132	240	−11	3.286	2.0	3.306	+0.020
GD 50	37	187	−39	1.805	22.	1.901	+0.096
GD 71	46.5	192	−05	2.414	2.0	3.145	+0.731
V471 Tau	46.8	172	−28	2.164	3.7	2.689	+0.525
α Aql	5.1	048	−9	3.468	3.6	3.068	−0.400
α PsA	7.7	020	−65	3.180	2.0	3.187	+0.007
α Cep	15.0	101	+09	2.837	3.5	3.049	+0.212
β Pic	19.3	258	−31	3.540	2.5	3.117	−0.423
δ Vel	24.4	272	−07	3.762	2.0	3.282	−0.480
δ Cas	30	127	−02	2.656	2.0	3.200	+0.544
α And	30	112	−33	1.797	12.	1.889	+0.092
α Gru	31	350	−52	3.574	2.7	3.167	−0.407
α Lac	31	101	−07	2.544	3.3	2.909	+0.365
α Peg	43	088	−40	2.546	3.4	2.700	+0.154
γ Aqr	48	062	−46	3.016	5.0	3.051	+0.035
η Aqr	56	067	−48	3.810	9.0	2.516	−1.294
η Aur	67	165	+00	2.644	2.0	3.322	+0.678

TABLE 4

COMPARISON OF LIC MODEL PARAMETERS

Property	Data Set A	Data Set B
HST stars used	16	16
EUVE stars used	01	03
Ca II stars used	00	13
Total	17	32
x_{center} (pc)	−2.2	−2.5
y_{center} (pc)	+1.2	+1.5
z_{center} (pc)	−1.1	−1.5
Reduced χ^2	0.56	1.33
Mean difference	0.14	0.28
Spherical Harmonic Coefficients		
$a_{0,-0}$	+9.381	+8.982
$a_{1,-0}$	−1.026	−0.607
$a_{1,-1}$	+0.532	−0.171
$a_{1,-1}$	+0.360	−0.046
$a_{2,-0}$	+0.622	+0.995
$a_{2,-1}$	−0.501	−0.913
$a_{2,-1}$	−0.414	+0.202
$a_{2,-2}$	−0.280	−0.309
$a_{2,-2}$	+1.589	+2.068

Figure 3 shows the LIC model based on data set B as seen from the Galactic center direction ($l = 0°$, $b = 0°$). The 0 pc contour shows the edge of the LIC in a plane perpendicular to the Galactic center direction that passes through the Sun. Positive and negative values refer to distances toward and away from the Galactic center.

Figure 4 shows the LIC model based on data set B from a third perspective, Galactic west ($l = 270°$, $b = 0°$).

Finally, we show in Figure 5 the location in Galactic coordinates of the *HST*, *EUVE*, and Ca II stars used in this analysis. The two-symbol designations for each star are listed in column (1) of Table 1. Also shown are contours (from darkest to lightest) of $N_{H\,I} = 2.0$, 1.0, 0.5, 0.25, 0.10, and 0.05×10^{18} cm^{-2} from the Sun to the edge of the LIC. These contours are useful for estimating hydrogen column densities through the LIC, and a tool is available at the Web site described below for computing more accurate column densities through the LIC. For example, in Paper I we could not determine whether the line of sight to ϵ Ind ($l = 336°$, $b = -48°$) passes through the LIC or the G cloud since the projected velocities of both clouds are the same in this direction. Using Figure 5, we infer a column density through the LIC, $N_{H\,I}^{LIC} < 0.05 \times 10^{18}$ cm^{-2}. Thus, essentially all of the line of sight to ϵ Ind passes through the G

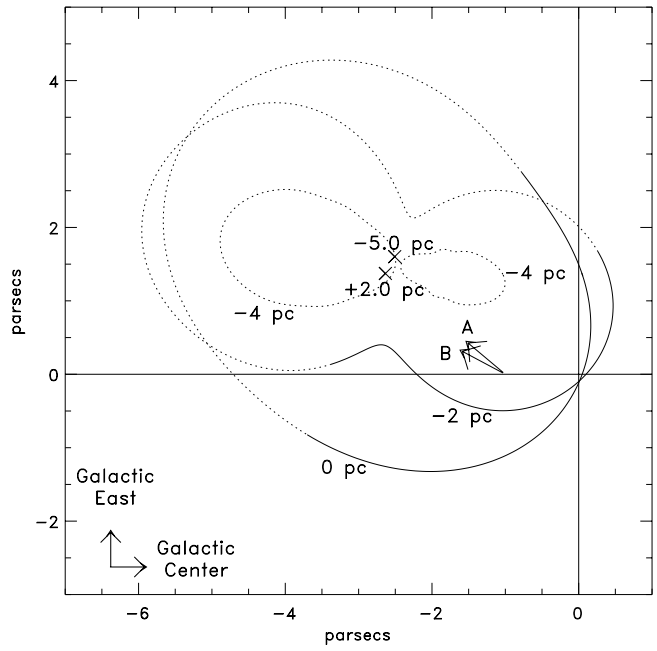

FIG. 2.—View from the north Galactic pole of the LIC model computed from hydrogen column densities inferred from *HST*, *EUVE*, and ground-based Ca II spectra (data set B). The Sun is located at (0, 0), and the directions toward the Galactic center ($l = 0°$) and Galactic east ($l = 90°$) are indicated. The 0 pc line is the LIC boundary in a plane parallel to the Galactic plane passing through the Sun. The −2 and −4 pc contours show the edge of the LIC in planes located at 2 and 4 pc south of the Sun. The northernmost point of the LIC at +2.0 pc and the southernmost point at −5.0 pc are both indicated by crosses. The solid portion of the contours indicate where the model is well constrained, as indicated by the averaging of models from various orientations. The dotted regions indicate where the model is poorly constrained. The arrow marked A indicates the direction from the center of the Sco-Cen association ($l = 320°$, $b = +15°$). The arrow marked B is the direction of the flow vector within the LIC in the local standard of rest ($l = 331.^{\circ}9$, $b = +4.^{\circ}6$).

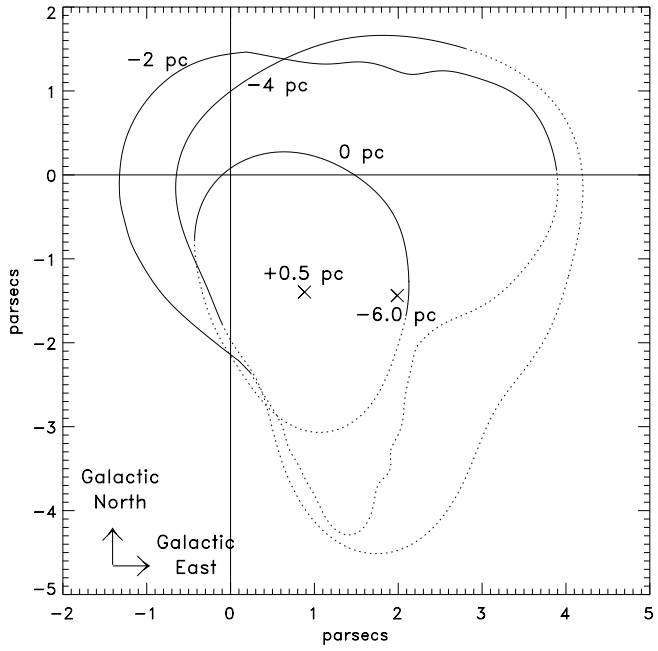

FIG. 3.—View from the Galactic center of the LIC model computed from hydrogen column densities inferred from *HST*, *EUVE*, and ground-based Ca II spectra (data set B). The Sun is located at (0, 0), and the directions toward Galactic east ($l = 90°$, $b = 0°$) and Galactic north ($b = 90°$) are indicated. The 0 pc line is the LIC boundary in a plane perpendicular to the Galactic center direction passing through the Sun. The −2 and −4 pc contours show the edge of the LIC in planes located at 2 and 4 pc behind the Sun (farther from the Galactic center). The edge of the LIC closest to the Galactic center (at +0.5 pc) and farthest from the Galactic center (−6.0 pc) are marked with crosses. The solid portion of the contours indicate where the model is well constrained, as indicated by the averaging of models from various orientations. The dotted regions indicate where the model is poorly constrained.

cloud. It is clear from Figure 5 that there are large regions where no data exist. As more data become available, our model will change, perhaps drastically in regions where no data currently exist. More accurate three-dimensional models of the LIC can be constructed using the methods in this paper as a prescription when more lines of sight are characterized.

2.5. *The Colorado Local Interstellar Medium Web Site*

Our model of the LIC with the GHRS, STIS, *EUVE*, and Ca II data is version 1999/8 of the Colorado Model of the Local Interstellar Cloud.[3] The input data, prescription for computing the model, and tools for calculating the hydrogen column density and LIC velocity in any direction are also available at this Web site. As new data appear and we can model other nearby warm clouds (Génova et al. 1997), updated versions of the LISM model will be placed at this Web site. We are providing this Web site as a service to those who wish to estimate interstellar absorption or other properties in or through the LIC.

3. DISCUSSION

3.1. *Morphology*

Until now we have made the very simplest assumptions concerning the structure of the LIC: all interstellar gas moving with a speed consistent with the LIC velocity vector has a constant density, $n_{\rm H\,I} = 0.10$ cm^{-3}, and this gas extends from the heliosphere to the edge of the LIC as determined by the value of $N_{\rm H\,I}$ for this velocity component along each line of sight. A very different picture has been put forward by Frisch & York (1983) and by Frisch (1996), who argue that the LISM consists of thin filaments or fluffy layers of warm gas that may be fragments of the shell of the Local Bubble. Thin filaments are commonly seen throughout the interstellar medium, for example, the Cygnus superbubble (Graham et al. 1995) or reflection nebulae in the Pleiades. Our model of the LIC has a minimum thickness of 4.7 pc and minimum hydrogen column density of 1.5×10^{18} cm^{-2} through the cloud. The maximum dimension is 6.8 pc, corresponding to $N_{\rm H\,I} = 2.1 \times 10^{18}$ cm^{-2}. We believe that our model is a good representation of the LIC because it is based primarily on measured hydrogen column densities in many lines of sight through the LIC for gas moving at the projected LIC velocity rather than hydrogen column densities integrated over all velocities.

Which model shape is more nearly correct? Are these extreme cases and the local interstellar gas structure lies somewhere between the two extremes? On the basis of Ca II interstellar spectra and extreme ultraviolet absorption in the spectra of 16 white dwarfs observed by *EUVE*, Frisch (1996) concluded that the local cloud complex (not just the LIC) is a filament with thickness ≤ 0.7 pc and crosswise hydrogen column density $\leq 2 \times 10^{17}$ cm^{-2}. This filamentary structure is inconsistent with our model. Part of the

[3] This model can be viewed at the Colorado Local Interstellar Medium Web site at http://casa.colorado.edu/~sredfiel/ColoradoLIC.html.

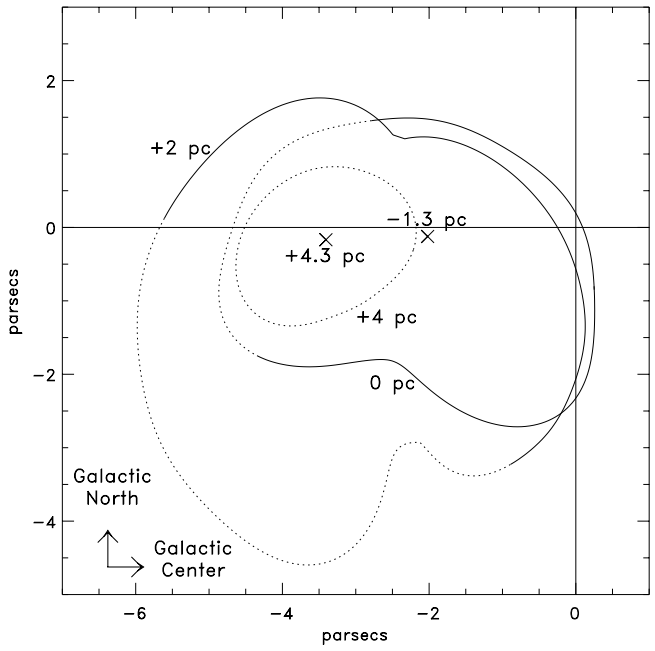

FIG. 4.—View from the Galactic west ($l = 270°$, $b = 0°$) direction of the LIC model computed from hydrogen column densities inferred from *HST*, *EUVE*, and ground-based Ca II spectra (data set B). The Sun is located at (0,0), and the directions toward the Galactic center ($l = 0°$, $b = 0°$) and Galactic north ($b = 90°$) are indicated. The 0 pc line is the boundary of the LIC in a plane perpendicular to the Galactic west direction passing through the Sun. The +2 and +4 pc contours show the edge of the LIC in planes located at 2 and 4 pc behind the Sun (toward the Galactic east direction). The edge of the LIC closest to the Galactic west direction (at −1.3 pc) and farthest from the Galactic west (at +4.3 pc) are marked with crosses. The solid portion of the contours indicate where the model is well constrained, as indicated by the averaging of models from various orientations. The dotted regions indicate where the model is poorly constrained.

difference may be due to the Sun being very close to the edge of the LIC. More data will help determine the nature of the shape of the LIC. If hydrogen column densities in unsampled sight lines are consistent with our model, the smooth-shaped LIC model is supported.

Our model does assume that the LIC gas is reasonably homogeneous in density. However, Meyer & Blades (1996) and Watson & Meyer (1996) demonstrated that the ISM can be inhomogeneous on subparsec scales on the basis of significantly different Na I interstellar absorption along the lines of sight toward the two components of visual binaries like μ Cru, where the separation is only 6600 AU (0.032 pc). Structures on this small scale have been seen, so far, only for cold gas in the ISM, not the warm gas traced by H I and D I. Until now we have had no reliable technique for assessing the inhomogeneity of the LIC, as the measured column densities only constrain the amount of material and not its distribution along a given line of sight. The interstellar column densities of H I, D I, and Mg II toward the only nearby binary system studied to date, α Cen A and B, are essentially the same within the measurement errors (Linsky & Wood 1996).

The discovery of hydrogen walls around the Sun and many nearby stars provides a new source of information that we can exploit to assess the inhomogeneity of the LIC. Wood & Linsky (1998) summarized the evidence for warm, decelerated neutral hydrogen in the upwind direction around the Sun, ϵ Eri, 61 Cyg A, ϵ Ind, 40 Eri A, and λ And. Vidal-Madjar et al. (1998) have now added Capella to the list of stars that show evidence for hydrogen walls. Since the presence of a hydrogen wall requires that the star be embedded in a partially ionized interstellar cloud, those lines of sight toward stars with hydrogen walls must have warm interstellar gas along both the beginning and the end of the line of sight. In Table 1 of Paper I, we underlined the names of the six stars for which hydrogen walls have now been identified. For these stars, $\langle n_{\rm H\,I} \rangle$ lies in the range 0.040–0.095 cm^{-3}. One possible conclusion is that these lines of sight are partly filled (with filling fractions in the range 0.40–0.95). An alternative conclusion is that the mean densities along lines of sight through the LIC vary by a factor of 2.5. In either case, the LIC appears to be inhomogeneous but not by a large factor.

As seen from the north Galactic pole, the LIC has an axis of symmetry that points in the direction $l \approx 320°$. Since the direction from the center of the Scorpius-Centaurus association is $l = 320°$ (Fig. 1*a*, *arrow A*), the shape of the LIC could be determined by the flow of hot gas from Sco-Cen.

The LIC model shows that the Sun is located just inside the edge in the direction of the Galactic center and toward the north Galactic pole. The LIC model also shows that there is very little LIC column density in the fourth ($270° < l < 360°$) and first ($0° < l < 90°$) Galactic quadrants. The proximity of the Sun to the edge of the LIC was previously noted by Lallement & Bertin (1992) and by Bertin et al. (1995). Most of the LIC volume lies east of the Galactic center in the second quadrant ($90° < l < 180°$). This distribution of LIC gas in the Galactic plane is the opposite of what is seen in the *total* hydrogen column density in previous studies. For example, Frisch & York (1983) and Paresce (1984) called attention to the relatively short distance to reaching log $N_{\rm H\,I} = 10^{19}$ cm^{-2} in the first and fourth Galactic quadrants and the $\geq$200 pc distance to this hydrogen column density contour in the third Galactic quadrant. Also, Vallerga (1996) showed that *EUVE* detected a relatively large number of white dwarfs in the third quadrant (indicating low hydrogen column densities) and very few white dwarfs in the direction of the Galactic center, especially for $b > 0°$. These results and others are consistent with very little hydrogen column density beyond the LIC in the third quadrant but a large hydrogen column beyond the LIC in the fourth and first quadrants in the G cloud.

The absence of Mg II absorption at the LIC velocity toward α Cen indicates that the distance to the edge of the LIC in this direction is $\leq$0.05 pc, and the Sun should cross the boundary between the LIC and the G cloud in less than 3000 yr.

We estimate that the volume of the LIC is about 93 pc^3 and its mass is about 0.32 $M_\odot$.

3.2. *Comparison with Theoretical Models*

We now compare the measured physical properties and morphology of the LIC with theoretical models. Table 5 lists our adopted empirical properties of the LIC and the references from which these data were taken. The value of the LIC temperature, derived from absorption line widths, is representative of many lines of sight through the LIC. The electron density refers only to the Capella line of sight for which we have a reliable value based on GHRS spectra,

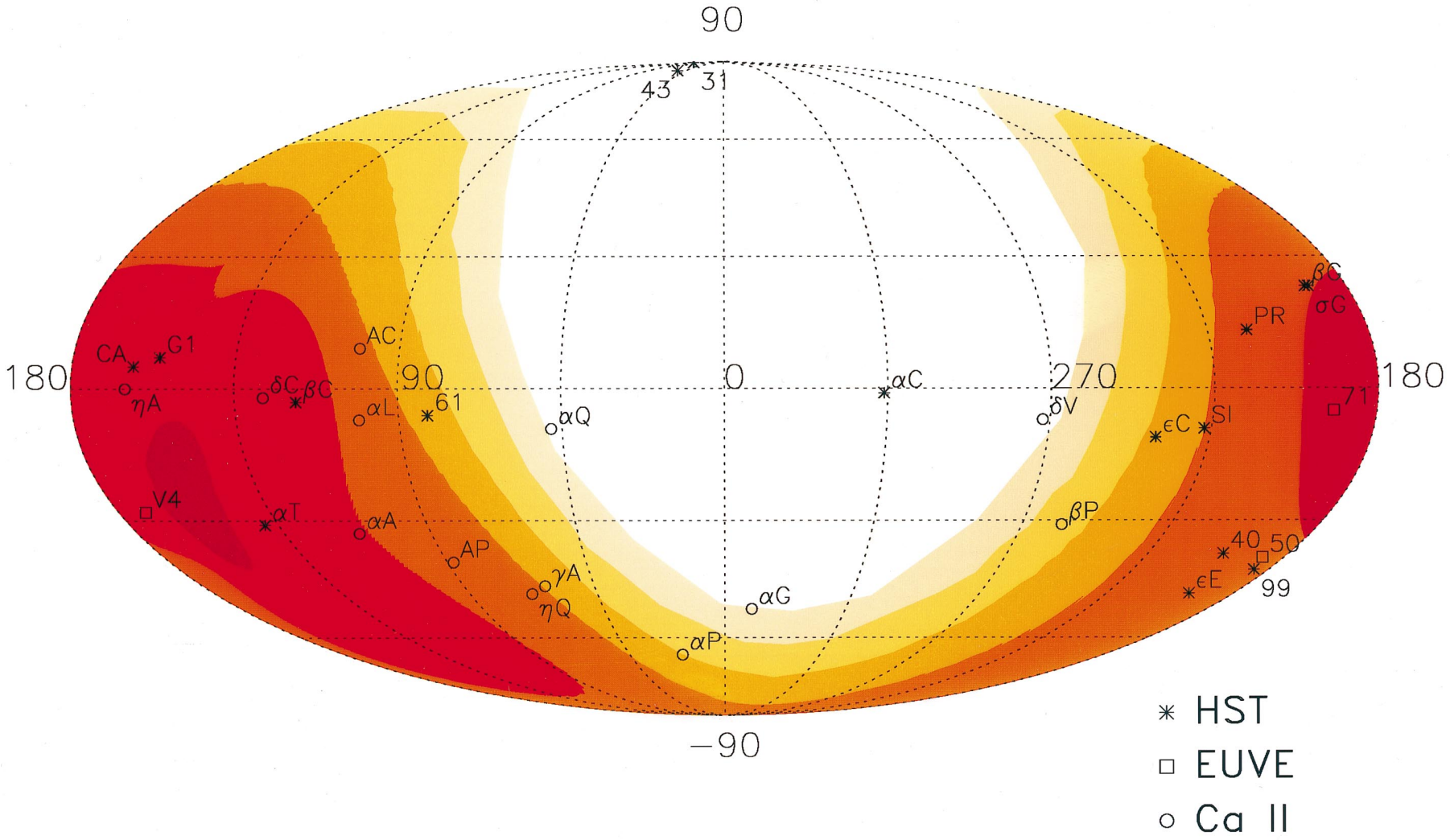

FIG. 5.—The location of the *HST*, *EUVE*, and Ca II stars used in this analysis are shown in Galactic coordinates. The symbols identifying the stars are listed in the first columns of Tables 1 and 2. The shadings indicate values of $N_{H\,I}$ in units of 10^{18} cm^{-2} from the Sun to the edge of the LIC, based on data set B. From darkest to lightest, the shadings designate greater than 2.0, 1.0–2.0, 0.5–1.0, 0.25–0.50, 0.10–0.25, 0.05–0.10, and less than 0.05 in these units.

TABLE 5

PHYSICAL AND MORPHOLOGICAL PROPERTIES OF THE LIC

Property	Value	Reference
Temperature	7000 ± 1000 K	1
Neutral hydrogen density ($n_{\rm H\,I}$)	0.10 cm^{-3}	2
Electron density (n_e)	$0.11^{+0.12}_{-0.06}$ cm^{-3}	3
Hydrogen ionization [X(H) = $n_p/(n_{\rm H\,I} + n_p)$]	0.52 ± 0.18	4
Gas pressure (P/k)	1620^{+1280}_{-630} cm^{-3} K	4
log (depletion of Mg), D(Mg)	-1.1 ± 0.2	1
log (depletion of Fe), D(Fe)	-1.27	5
log (depletion of O), D(O)	-0.25	5
Maximum dimension	6.8 pc	6
Minimum dimension	4.7 pc	6
Maximum $N_{\rm H\,I}$	2.1×10^{18} cm^{-2}	6
Minimum $N_{\rm H\,I}$	1.5×10^{18} cm^{-2}	6

REFERENCES.—(1) Piskunov et al. 1997; (2) Paper I; (3) Wood & Linsky 1997; (4) computed; (5) Linsky et al. 1995; (6) this paper.

but Holberg et al. (2000) find a very similar value, $n_e = 0.11^{+0.07}_{-0.06}$ cm^{-3}, for the 132 pc line of sight to REJ 1032+535 using the same technique, and the high fractional ionization of hydrogen is consistent with the analysis of *EUVE* spectra toward many hot white dwarfs (Vallerga 1996). The most recent set of detailed models of the multiphase ISM were computed by Wolfire et al. (1995a). Their time-independent models assume pressure equilibrium between the CNM and WNM phases and ionization equilibrium within each phase. In the WNM phase, photoelectric heating from polycyclic aromatic hydrocarbons is balanced by cooling by Lyα, C II (158 μm), and O I (63 μm) radiation and by electron recombinations onto positively charged grains. They compute the temperature, density, and pressure for a standard model with attenuation of illuminating radiation by $N_{\rm H\,I} = 10^{19}$ cm^{-2} and solar abundances, but they also compute a range of models for different column densities, abundances, and grain sizes.

For the standard model, a neutral hydrogen density, $n_{\rm H\,I} = 0.10$ cm^{-3}, corresponds to a thermal gas pressure $P/k \approx 1000$ cm^{-3} K. The empirical parameters for our LIC model correspond to $P/k = 1.1(n_{\rm H\,I} + n_e)T = 1620^{+1280}_{-630}$ cm^{-3} K, which is similar to the value $P/k = 1700$–2300 cm^{-3} K estimated by Vallerga (1996) from *EUVE* spectra. The relation between P/k and $n_{\rm H\,I}$ is essentially unchanged for values of $n_{\rm H\,I}$ near 0.1 cm^{-3} when the assumed column density is decreased to $N_{\rm H\,I} = 10^{18}$ cm^{-2}, the gas-phase abundances are changed by a large factor, and the far-UV radiation field is changed by several orders of magnitude. In the Wolfire et al. (1995a) models, P/k decreases appreciably for fixed $n_{\rm H\,I}$ only when the grain abundances are far below solar, while the gas-phase abundances are solar. An interesting result is that for $P/k < 990$ cm^{-3} K with $N_{\rm H\,I} = 10^{19}$ cm^{-2} and for $P/k < 1600$ cm^{-3} K with $N_{\rm H\,I} = 10^{18}$ cm^{-2} only the WNM phase is possible. Thus, the gas pressure in the LIC is close to the limit where the CNM phase cannot exist.

The empirical hydrogen ionization, however, is much larger than in the Wolfire et al. theoretical models. For $n_{\rm H\,I} = 0.10$ cm^{-3}, the theoretical models predict that the $n_e/n_{\rm H\,I}$ ratio lies in the range 0.046–0.11 cm^{-3}, whereas the empirical ratio is 0.6–2.3. There is no set of parameters in the ionization equilibrium WNM models of Wolfire et al. (1995a) or in the WIM models for the Galactic halo (Wolfire et al. 1995b) that has this high degree of ionization for $n_{\rm H\,I} = 0.10$ cm^{-3}.

Vallerga (1998) computed the ionization equilibrium of hydrogen and helium in the LIC, including the extreme ultraviolet radiation from all sources detected by the *EUVE* satellite. Since the rather soft radiation from ϵ CMa dominates the photoionization of hydrogen, the LIC is self-shielding and the computed hydrogen ionization decreases from the LIC edge facing ϵ CMa toward the cloud interior. Vallerga computed a mean electron density $n_e = 0.068$ cm^{-3} in the direction of ϵ CMa. Thus, the measured value of $n_e = 0.11^{+0.12}_{-0.06}$ cm^{-3} toward Capella through the center of the LIC with $N_{\rm H\,I} = 1.9 \times 10^{18}$ cm^{-2} is inconsistent with the Vallerga photoionization equilibrium calculation, and the observed ionization of helium is even further in disagreement. We conclude that additional ionization or departures from ionization equilibrium are needed to explain the observed LIC ionization.

Two very different models have been proposed to account for the extra ionization. Frisch & Slavin (1996) and Slavin & Frisch (1998) proposed that the LIC is in steady state ionization equilibrium for which ionizing radiation from an evaporative boundary between the warm LIC and hot surrounding gas in the Local Bubble, together with radiation from nearby hot stars, can explain the observed high degree of hydrogen and helium ionization. Lyu & Bruhweiler (1996) described a very different model in which the ionization is far out of equilibrium. They argued that the high degree of ionization of hydrogen and especially helium in the warm LISM is due to the gas being in a recombination phase following complete ionization by shocks from a nearby supernova. Using their time-dependent ionization/recombination models, Lyu & Bruhweiler were able to fit the observed ionization of helium and hydrogen for the LISM gas with $n_{\rm H\,I} = 0.10$ cm^{-3} when the ionizing event occurred one or several million years ago. Rapid cooling after this ionizing event would lead to $T \approx 10^4$ K at the present time despite the overionization of the dominant species in the gas.

Since the rate of cooling in the important fine-structure lines of O I and C II is proportional to electron density, the overionization of hydrogen should make the LIC cooler than the ionization equilibrium models predict. We asked M. Wolfire (1999, private communication) to compute the

equilibrium temperature for $P/k = 1600$ cm^{-3} K and $N_{\rm H\,I} = 10^{18}$ or 10^{19} cm^{-2} using the latest version of his codes that assume ionization equilibrium. He computed $T = 9380$ K, whereas the empirical LIC temperature is $T = 7000 \pm 1000$ K. Since the ionization equilibrium theoretical models predict $n_e = 0.015$ cm^{-3}, the overionization factor is large, $7.3^{+8.0}_{-4.0}$.

M. Wolfire (1999, private communication) then kindly ran an updated version of his code (to be described in a forthcoming paper) with the following parameters: $n_{\rm H\,I} = 0.10$ cm^{-3}, $n_e = 0.11$ cm^{-3} (the empirical value), $N_{\rm H\,I} = 1.0 \times 10^{18}$ cm^{-2} and $N_{\rm H\,I} = 2.0 \times 10^{18}$ cm^{-2}, total gas-phase abundance of oxygen $n_{\rm O}/n_{\rm H} = 3.0 \times 10^{-4}$, $n_{\rm O\,I}/n_{\rm H} = 1.5 \times 10^{-4}$, and $n_{\rm C\,II}/n_{\rm H} = 1.4 \times 10^{-4}$. For this nonequilibrium ionization case, he computed $T = 6900$ K for $N_{\rm H\,I} = 1.0 \times 10^{18}$ cm^{-2} and $T = 6594$ K for $N_{\rm H\,I} = 2.0 \times 10^{18}$ cm^{-2}. These theoretical temperatures are in remarkable agreement with the observed values. Thus, the observed overionization and low temperature of the LIC are consistent with detailed energy balance calculations.

4. CONCLUSIONS

In this second paper in a series on the structure of the LISM, we construct a three-dimensional model of the LIC based on GHRS, STIS, *EUVE*, and ground-based Ca II spectra. Subsequent papers will refine this model by including new data and constructing models for other nearby clouds in the LISM. The following summarizes our findings to date:

1. We adopt the technique described in Paper I in which we determine the distance to the edge of the LIC, $d_{\rm edge}$(LIC), along a given line of sight from the hydrogen column density (inferred from the deuterium column density in GHRS spectra). We assume that the interstellar gas moving with the LIC speed has a constant density, $n_{\rm H\,I} = 0.10$ cm^{-3}, and the LIC extends from the heliosphere to an edge determined by the value of $N_{\rm H\,I}$(LIC) along each line of sight.

2. We first fit spherical harmonics to the 16 lines of sight for which we have values of $d_{\rm edge}$(LIC) or upper limits from the *HST* data. In the case of upper limits, we set $d_{\rm edge}$(LIC) equal to the upper limit. We can construct an orientation-averaged, three-dimensional model of the LIC to fit all of these data, with very little scatter (reduced $\chi^2 = 0.56$) and a smooth structure between the fitted points. By averaging the results of three different orientations, we obtain the most general solution to the three-dimensional structure of the LIC, as well as determine which regions are well constrained or poorly constrained.

3. We next considered whether the hydrogen column densities toward the white dwarfs observed by *EUVE* are consistent with the LIC shape determined only with the GHRS data. Since the *EUVE* hydrogen column densities refer to the absorption by all clouds in the line of sight, we do not know a priori whether the lines of sight to any of these stars only pass through the LIC. The value of $d_{\rm edge}$ for only one of the *EUVE* targets (GD 50) is consistent with the LIC shape. For this nearby star (37 pc), $N_{\rm H\,I}$(total) is similar to the values of $N_{\rm H\,I}$(LIC) for the stars HR 1099, ϵ Eri, and 40 Eri A that lie between 3°.4 and 11° from GD 50 on the sky. We therefore include GD 50 in our list of lines of sight and rederive the LIC shape.

4. We then considered lines of sight for which absorption in the Ca II resonance lines is observed at the projected LIC velocity. The conversion from Ca II column densities to hydrogen column densities requires knowledge of the Ca II/H I ratio that can vary from cloud to cloud. We find that a mean ratio, $N_{\rm Ca\,II}/N_{\rm H\,I} = 2.30^{+0.53}_{-0.28} \times 10^{-8}$, leads to the best fit of 13 Ca II lines of sight with the model based on the 16 *HST* and one *EUVE* data points. We therefore include these 13 Ca II lines of sight and recompute a model with nine spherical harmonics. At this time we also included two additional hot white dwarfs observed by *EUVE* as their total hydrogen column densities are smaller than predicted by the first LIC model and thus constrain the morphology of the LIC. The reduced $\chi^2 = 1.33$. Since the models computed with and without the Ca II lines of sight are in very good agreement, we now include Ca II column densities in models for the LIC and other nearby warm clouds. Our model of the LIC with the Ca II data is version 1999/8 of the Colorado Model of the Local Interstellar Cloud.

5. The LIC model is clearly not a long thin filamentary structure as optical images of some interstellar clouds (e.g., reflection nebulae in the Pleiades), but neither is it spherical in shape. As seen from the north Galactic pole, the LIC has an axis of symmetry that points in the direction $l \approx 315°$. Since the direction of the center of the Sco-Cen association is $l = 320°$, the shape of the LIC could be determined by the flow of hot gas from Sco-Cen.

6. The LIC model shows that the Sun is located just inside the edge in the direction of the Galactic center and toward the north Galactic pole. The absence of Mg II absorption at the LIC velocity toward α Cen indicates that the distance to the edge of the LIC in this direction is ≤ 0.05 pc and the Sun should cross the boundary between the LIC and the G cloud in less than 3000 yr.

7. We estimate that the volume of the LIC is about 93 pc^3 and its mass is about 0.32 $M_\odot$.

8. The physical parameters and hydrogen column density of the LIC are roughly consistent with the Wolfire et al. (1995a) warm ISM models that assume pressure and ionization equilibrium, but the empirical hydrogen ionization is much higher and the gas temperature lower than the theoretical models predict. The high ionization is naturally explained by the LIC gas being in a recombining phase following shock ionization from a nearby supernova as proposed by Lyu & Bruhweiler (1996). The higher ionization increases the gas cooling, which can explain why the gas is 2400 K cooler than the ionization equilibrium models predict. Computed and observed temperatures are remarkably in agreement for a theoretical model with the observed LIC electron density.

9. The LIC model can be seen at the Colorado Model of the Local Interstellar Medium Web site (see footnotes 2 and 3). The input data, prescription for computing the model, and a tool for calculating the hydrogen column density in any direction will also be at this Web site. As new data appear and we can model other warm clouds, updated versions of the LISM model will be placed on this Web site.

Many questions still remain concerning the structure of the LISM. For example, only a few of the perhaps many clouds near the Sun have been identified so far, and there are few data on the hydrogen absorption through the G cloud. Whether these structures that we call "clouds" are actually individual parcels of gas with long-term identities, transient shock fronts, or turbulent eddies remains to be

TABLE 6

SPHERICAL HARMONIC BASIS FUNCTIONS

Harmonic	Normalized Functional Form
$y_{0,0}$	$\sqrt{\frac{1}{4\pi}}$
$y_{1,0}$	$\sqrt{\frac{3}{4\pi}} \cos\theta$
$y_{1,-1}$	$\sqrt{\frac{3}{4\pi}} \sin\theta \cos\phi$
$y_{1,1}$	$\sqrt{\frac{3}{4\pi}} \sin\theta \sin\phi$
$y_{2,0}$	$\sqrt{\frac{5}{16\pi}} (3\cos^2\theta - 1)$
$y_{2,-1}$	$\sqrt{\frac{15}{4\pi}} \sin\theta \cos\theta \cos\phi$
$y_{2,1}$	$\sqrt{\frac{15}{4\pi}} \sin\theta \cos\theta \sin\phi$
$y_{2,-2}$	$\sqrt{\frac{15}{16\pi}} \sin^2\theta \cos 2\phi$
$y_{2,2}$	$\sqrt{\frac{15}{16\pi}} \sin^2\theta \sin 2\phi$

determined. We do not yet know whether the cloud boundaries on subarcsecond scales are smooth, as suggested by our models computed using spherical harmonics, or very irregular with embedded small high-density clouds. Also, are densities fairly uniform within a given cloud or inhomogeneous? Considerably more high-quality data are needed to sort out these important questions.

This work is supported by NASA grant S-56460-D to the National Institute of Standards and Technology. We thank Mark Wolfire for kindly computing theoretical models with our input parameters and Richard McCray and Mike Shull for their comments and suggestions. We would also like to thank the referee for providing thoughtful and important suggestions.

APPENDIX

Any arbitrary function $r(\theta, \phi)$ can be expanded in a series of spherical harmonics:

$$d_{\rm edge}(\theta, \phi) = \sum_{l=0}^{\infty} \sum_{m=-l}^{l} a_{l,m} Y_{l,m}(\theta, \phi) , \tag{A1}$$

where $a_{l,m}$ are real, constant coefficients associated with a specific, complex spherical harmonic $Y_{l,m}$. In our case, we are concerned only with real surface quantities, so it is more convenient to work with real spherical harmonics $y_{l,m}$, where

$$y_{l,m}(\theta, \phi) = \begin{cases} \frac{1}{\sqrt{2}} [Y_{l,m}(\theta, \phi) + Y^*_{l,m}(\theta, \phi)] & \text{if} \quad m > 0, \\ Y_{l,0}(\theta, \phi) & \text{if} \quad m = 0, \\ \frac{-i}{\sqrt{2}} [Y_{l,|m|}(\theta, \phi) - Y^*_{l,|m|}(\theta, \phi)] & \text{if} \quad m < 0. \end{cases} \tag{A2}$$

The complex spherical harmonics $Y_{l,m}(\theta, \phi)$ [and its complex conjugate $Y^*_{l,m}(\theta, \phi)$] are related to associated Legendre polynomials and can be recursively generated in a straightforward fashion (Jackson 1999; Press et al. 1992). The normalization of the real spherical harmonics, $y_{l,m}$, is such that $\int y^2_{l,m}(\theta, \phi) d\Omega = 1$. We make all constants of normalization positive and allow the fit coefficients $a_{l,m}$ to carry the appropriate sign. The real spherical harmonics with proper normalizations for $l = 0, 1, 2$ are given in Table 6. The only quantities that are unknown in the function (A1) are the $a_{l,m}$ coefficients. Our task is to determine those coefficients that best describe the three-dimensional shape of the LIC.

REFERENCES

Bertin, P., Vidal-Madjar, A., Lallement, R., Ferlet, R., & Lemoine, M. 1995, A&A, 302, 889
Cox, D. P., & Reynolds, R. J. 1987, ARA&A, 25, 303
Cox, D. P., & Smith, B. W. 1974, ApJ, 189, L105
Crawford, I. A. 1991, A&A, 247, 183
Crawford, I. A., & Dunkin, S. K. 1995, MNRAS, 273, 219
Ferlet, R., Lallement, R., & Vidal-Madjar, A. 1986, A&A, 163, 204
Field, G. B., Goldsmith, D. W., & Habing, H. J. 1969, ApJ, 155, L149
Frisch, P. C. 1995, Space Sci. Rev., 72, 499
———. 1996, Space Sci. Rev., 78, 213
Frisch, P. C., & Slavin, J. D. 1996, Space Sci. Rev., 78, 223
Frisch, P. C., & York, D. G. 1983, ApJ, 271, L59

Génova, R., Beckman, J. E., Bowyer, S., & Spicer, T. 1997, ApJ, 484, 761
Graham, J. R., Levenson, N. A., Hester, J. J., Raymond, J. C., & Petre, R. 1995, ApJ, 444, 787
Holberg, J. B., Bruhweiler, F. C., Barstow, M. A., & Dobbie, P. D. 2000, ApJ, in press
Jackson, J. D. 1999, Classical Electrodynamics (3d ed.; New York: Wiley)
Lallement, R., & Bertin, P. 1992, A&A, 266, 479
Lallement, R., Ferlet, R., Lagrange, A. M., Lemoine, M., & Vidal-Madjar, A. 1995, A&A, 304, 461
Lallement, R., Vidal-Madjar, A., & Ferlet, R. 1986, A&A, 168, 225
Linsky, J. L., Diplas, A., Wood, B. E., Brown, A., Ayres, T. R., & Savage, B. D. 1995, ApJ, 451, 335
Linsky, J. L., Redfield, S., Piskunov, N., & Wood, B. E. 2000, ApJ, 528, 756 (Paper I)
Linsky, J. L., & Wood, B. E. 1996, ApJ, 463, 254
Lyu, C.-H., & Bruhweiler, F. C. 1996, ApJ, 459, 216
McKee, C. F. 1995, in ASP Conf. Ser. 80, The Physics of the Interstellar Medium and Intergalactic Medium, ed. A. Ferrara, C. F. McKee, C. Heiles, & P. R. Shapiro (San Francisco: ASP), 292
Meyer, D. M., & Blades, J. C. 1996, ApJ, 464, L179
Paresce, F. 1984, AJ, 89, 1022
Piskunov, N., Wood, B. E., Linsky, J. L., Dempsey, R. C., & Ayres, T. R. 1997, ApJ, 474, 315
Press, W., Teukolsky, S. A., Vetterling, W. T., & Flannery, B. P. 1992, Numerical Recipes: The Art of Scientific Computing (2d ed.; New York: Cambridge Univ. Press)
Slavin, J. D., & Frisch, P. C. 1998, in The Local Bubble and Beyond, ed. D. Breitschwerdt, M. J. Freyberg, & J. Truemper (Berlin: Springer), 305
Vallerga, J. 1996, Space Sci. Rev., 78, 277
———. 1998, ApJ, 497, 921
Vallerga, J. V., Vedder, P. W., Craig, N., & Welsh, B. Y. 1993, ApJ, 411, 729
Vidal-Madjar, A., Lemoine, M., Ferlet, R., Hébrard, G., Koester, D., Audouze, J., Cassé, M., Vangioni-Flam, E., & Webb, J. 1998, A&A, 338, 694
Watson, J. K., & Meyer, D. M. 1996, ApJ, 473, L127
Welty, D. E., Morton, D. C., & Hobbs, L. M. 1996, ApJS, 106, 533
Wolfire, M. G., Hollenbach, D., McKee, C. F., Tielens, A. G. G. M., & Bakes, E. L. O. 1995a, ApJ, 443, 152
Wolfire, M. G., McKee, C. F., Hollenbach, D., & Tielens, A. G. G. M. 1995b, ApJ, 453, 673
Wood, B. E., & Linsky, J. L. 1997, ApJ, 474, L39
———. 1998, ApJ, 492, 788